

Original Article

Cite this article: Blaise T, Ali Khoudja SA, Carpentier C, Brigaud B, Missenard Y, Mangenot X, Boulvais P, Landrein P, and Cochard J (2023) Far-field brittle deformation record in the eastern Paris Basin (France). *Geological Magazine* **159**: 2095–2109. <https://doi.org/10.1017/S0016756822000772>

Received: 10 December 2021
Revised: 30 June 2022
Accepted: 2 July 2022
First published online: 14 October 2022








Keywords:

calcite U–Pb geochronology; Jurassic limestones; Paris Basin; tension gash; far-field deformation

Author for correspondence:

Thomas Blaise,
Email: thomas.blaise@universite-paris-saclay.fr

Far-field brittle deformation record in the eastern Paris Basin (France)

Thomas Blaise¹ , Sid Ahmed Ali Khoudja¹, Cédric Carpentier² , Benjamin Brigaud¹ , Yves Missenard¹ , Xavier Mangenot³ , Philippe Boulvais⁴ , Philippe Landrein⁵  and Jean Cochard⁵

¹Université Paris-Saclay, CNRS, GEOPS, Orsay 91405, France; ²Université de Lorraine, CNRS, GeoRessources, Nancy 54500, France; ³Caltech, Geological and Planetary Sciences, Pasadena, CA 91106, USA; ⁴Géosciences Rennes, CNRS, Univ. Rennes, UMR 6118, Rennes F35000, France and ⁵Centre de Meuse/Haute-Marne, Agence Nationale pour La Gestion des Déchets Radioactifs (ANDRA), RD 960, Bure 55290, France

Abstract

Jurassic carbonate strata in the eastern Paris Basin exhibit several generations of faults, tension gashes and stylolites. Although their relative chronology can sometimes be determined according to cross-cutting relationships, the duration of major deformation phases and their influence on fluid flow and carbonate cementation are still uncertain. This contribution aims to clarify the timing of brittle deformation and associated calcite cementation. Tension gashes filled by calcite in Jurassic carbonates were sampled in outcrops and boreholes and dated through U–Pb geochronology. Almost all the sampled fractures were cemented during the Cenozoic period. Continuous deformation spread from *c.* 50 to 30 Ma. Tension gashes oriented N10° to N20° dated at 48–43 Ma show the main Pyrenean contractional stage. A second set of calcites were dated at *c.* 35–33 Ma and document a Late Eocene – Oligocene extension. A transition from the compressional to the extensional regime is expressed by tension gashes dated between 43 and 35 Ma. Finally, tension gashes oriented N150° to N175°, dated between 32 and 18 Ma, may result from the propagation of the horizontal stress generated by the Alpine orogen or by late Pyrenean deformation. Clumped isotope thermometry on five samples revealed both low crystallization temperatures (from 27 to 53 °C) and the meteoric origin of calcite-precipitating fluids. Our research therefore documents a continuous fracturing from Ypresian to Rupelian times, and less expressed brittle deformation during the Miocene period.

1. Introduction

Plate interiors can record far-field deformation as a consequence of tectonic events at their boundaries (e.g. Lacombe *et al.* 1996; Lacombe & Mouthereau, 1999). The propagation of stress regimes within the intraplate domain may result in long-wavelength folding, reactivation of existing discontinuities, differential erosion of tilted blocks and the development of faults, joints, tension gashes or stylolites, especially in sedimentary strata of intracratonic basins (e.g. Bergerat, 1987; Lacombe & Obert, 2000; Parrish *et al.* 2018). In carbonate rocks, these deformation patterns may enhance fluid flow in permeable strata and favour calcite dissolution–recrystallization, the cementation of primary intergranular porosity or the creation of a secondary pore space (e.g. Bruna *et al.* 2013). Such far-field deformations have long been recognized in the European plate, and palaeostress reconstructions were proposed using the inversion of fault slip data or the orientation of calcite twins (e.g. Lacombe *et al.* 1990).

In the context of radioactive waste storage within sedimentary rocks, the knowledge of the precise chronology of palaeostress fields is essential to understand the development of fracture networks and the self-sealing capacities of the sedimentary system (e.g. Sutcliffe *et al.* 2020). It also brings a source of valuable information regarding the palaeo-fluid flow in carbonates and the potential advective flows within claystones (Mazurek *et al.* 2018; Pagel *et al.* 2018). In the eastern Paris Basin, tectonic markers have been investigated in detail within and around the Underground Research Laboratory (URL) of the French National Agency for Radioactive Waste Management (Andra) (André *et al.* 2010 and references therein). All studies converge in demonstrating that most of the brittle deformation has developed during Cenozoic times. Defining the succession of palaeostress regimes from microtectonic analyses in this area is, however, complicated owing to many uncertainties. The relationship between a tectonic marker and a corresponding deformation event can indeed be ambiguous (e.g. in the eastern Paris Basin, bedding stylolites have developed both during sedimentary burial and in response to extensional stresses during Eocene–Oligocene times, while this portion of the basin was subjected to inversion; André *et al.* 2010). The cross-cutting relationships and the relative chronology of tectonic features are sometimes unclear (André *et al.* 2010; Vandeginste *et al.* 2012; Hoareau *et al.* 2021).

If the same palaeostress regime occurred during distinct deformation events, the orientation of tectonic markers may fail to provide genetic information. For instance, in the eastern Paris Basin, NW–SE compression may either be attributed to Late Cimmerian Unconformities (Guillocheau *et al.* 2000) during the Jurassic/Cretaceous transition or to Alpine compression during the Miocene period (André *et al.* 2010). Moreover, the orientation of the main stress axes rotated through time during the propagation of contractional deformation related to the Pyrenean and Alpine orogens (André *et al.* 2010).

Based on the orientation of tension gashes and the petrogeochemical characteristics of calcite filling fractures, vugs and intergranular pore spaces, Carpentier *et al.* (2014) proposed a conceptual cementation model for the Middle and Upper Jurassic carbonates in the eastern Paris Basin. The synthetic paragenetic sequence of Carpentier *et al.* (2014) is based on relative chronologies of cements, fractures and stylolites, together with the correlation of several petrogeochemical characteristics of calcite cements, including cathodoluminescence, major and trace elemental concentrations, and on oxygen and carbon stable isotope compositions. Such correlations should, however, be taken with caution, since all these properties are controlled by the physical-chemical parameters prevailing locally during calcite precipitation, such as the temperature, the intensity of fluid–rock interaction and the fluid/rock ratio, the elemental and isotopic composition of calcite-crystallizing fluids, and finally the vertical and lateral variations in the diagenetic medium (pore sizes, presence of stylolites, composition of the host carbonate rocks).

By contrast, calcite U–Pb geochronology constitutes a far more robust tool to provide absolute temporal correlation of cementation phases and their genetic relationship to large-scale brittle deformation events (Beaudoin *et al.* 2018; Hansman *et al.* 2018; Lawson *et al.* 2018; Roberts *et al.* 2020). So far, three U–Pb ages in calcite cement filling either vugs or fractures were evidenced in the studied area using either isotope dilution thermal ionization mass spectrometry (TIMS) (Pisapia *et al.* 2018) or laser ablation inductively coupled plasma mass spectrometry (LA-ICP-MS) (Pagel *et al.* 2018; Brigaud *et al.* 2020). The first age is *c.* 150 Ma, found exclusively in the Middle Jurassic limestones. The second and third ages are *c.* 43 Ma and 33 Ma, respectively. Although these ages offer a better understanding of the cementation events within the studied area, their link with geodynamic events, the duration of deformation (episodic versus continuous) and the relationship with palaeostress regimes remain uncertain. Moreover, the absence of calcite cement younger than *c.* 33 Ma puts into question the role of the Alpine orogen located closer to the investigated area when compared to the Pyrenean front. Finally, the origin of fluids involved in calcite precipitation in fractures, vugs or in the intergranular pore space still requires further investigation. The oxygen stable isotope composition of calcite in tension gashes was systematically measured by André *et al.* (2010), but the nature of mineralizing fluid was not fully resolved because crystallization temperatures were not known.

In this contribution, we integrated *in situ* U–Pb geochronology with clumped isotope thermometry in calcite-filled tension gashes, hydraulic breccias and intergranular pore space to constrain the origin, impact and duration of the main deformation phases that affected the eastern Paris Basin. We discuss the nature and temperature of calcite parent fluids and the impact of brittle structures on the cementation of the Middle and Upper Jurassic limestones. We compare our ages obtained on calcite cements with those documented by previous authors in the Paris Basin (Mangenot *et al.*

2018; Pagel *et al.* 2018; Pisapia *et al.* 2018; Brigaud *et al.* 2020) and in the northern and southern Pyrenees (Cruset *et al.* 2020; Parizot *et al.* 2021, respectively). Our results contribute to the understanding of the relationship between intraplate deformation and the cementation of carbonate rocks in intracratonic sedimentary basins.

2. Geological setting

A detailed view of the facies and diagenesis in the Jurassic strata of the eastern Paris Basin is given in Brigaud *et al.* (2014) and Carpentier *et al.* (2014). A succession of blocky calcite phases was evidenced that precipitated either during burial (Vincent *et al.* 2007; Brigaud *et al.* 2020) or during the inversion phase that occurred throughout the Cenozoic period (Buschaert *et al.* 2004; Pagel *et al.* 2018; Brigaud *et al.* 2020; Blaise *et al.* 2022). Blocky calcite of Cenozoic ages precipitated from meteoric fluids (Buschaert *et al.* 2004) and displays a typical dull brown cathodoluminescence (Carpentier *et al.* 2014). Below, we will first focus on the sedimentary cycles and facies of the Middle and Upper Jurassic limestones, and subsequently on major faults and palaeostress regimes.

The Lower Bajocian consists of ~30 m thick bioclastic limestones together with bioherms, called the *Calcaires à Polypiers* Formation (Durllet & Thierry, 2000; Brigaud *et al.* 2014), changing to marly sedimentation during the Early/Late Bajocian transition (*Marnes de Longwy* Formation). A new carbonate ramp then developed in the northeastern Paris Basin from Late Bajocian to Early Callovian times, with a typical inner ramp depositional environment (oolitic shoal or lagoon: *Oolites miliaire* and *Calcaires de Chaumont* formations) at the origin of ~150 m thick oolitic, bioclastic or mud-dominated limestones (Brigaud *et al.* 2009). A general flooding of the platform resulting in the deposition of locally thick (>100 m) clay-rich sediments started during Callovian time and lasted until Early Oxfordian time. The carbonate sedimentation started again during Middle Oxfordian time, with ~150 m thick reefal-dominated limestones (*Complexe récifal* Formation) and oolitic limestones (*Oolithe de Lamothé* and *Oolithe de Saucourt* formations; Brigaud *et al.* 2014). Flooding of the platform coeval with a climate cooling (Olivier *et al.* 2004; Carpentier *et al.* 2007; Brigaud *et al.* 2008) favoured a decrease in the carbonate production and the increase of siliciclastic inputs at the beginning of Late Oxfordian time with the deposition of the *Argiles à huitres* (Carpentier *et al.* 2010; Brigaud *et al.* 2014). A major carbonate production crisis occurred during the Oxfordian/Kimmeridgian transition (Lefort *et al.* 2011), with marl-dominated sedimentation (*Marnes à Exogyres* Formation), followed by a mixed carbonate, evaporite and siliciclastic ramp environment during Tithonian time (Brigaud *et al.* 2018).

The major tectonic discontinuities in the eastern Paris Basin are reported in Figure 1. A detailed description of the main fault systems can be found in Le Roux (1980), Bergerat *et al.* (2007) and André *et al.* (2010). Some faults correspond to Variscan sutures that later were reactivated during Meso-Cenozoic times, such as the E–W Vittel fault, the E–W to NE–SW Metz fault and the NNW–SSE to NW–SE Marne fault. By contrast, the NNE–SSW Gondrecourt and Joinville grabens are rooted within the Keuper halite Formation and did not propagate through the basement. These symmetric troughs are related to the European Cenozoic Rift System (ECRIS; Coulon, 1992; Ziegler & Dèzes, 2007; Ring & Gerdes, 2016). Roughly perpendicular to the Gondrecourt graben, the Poissons fault system constitutes the western border of the area currently investigated by Andra.

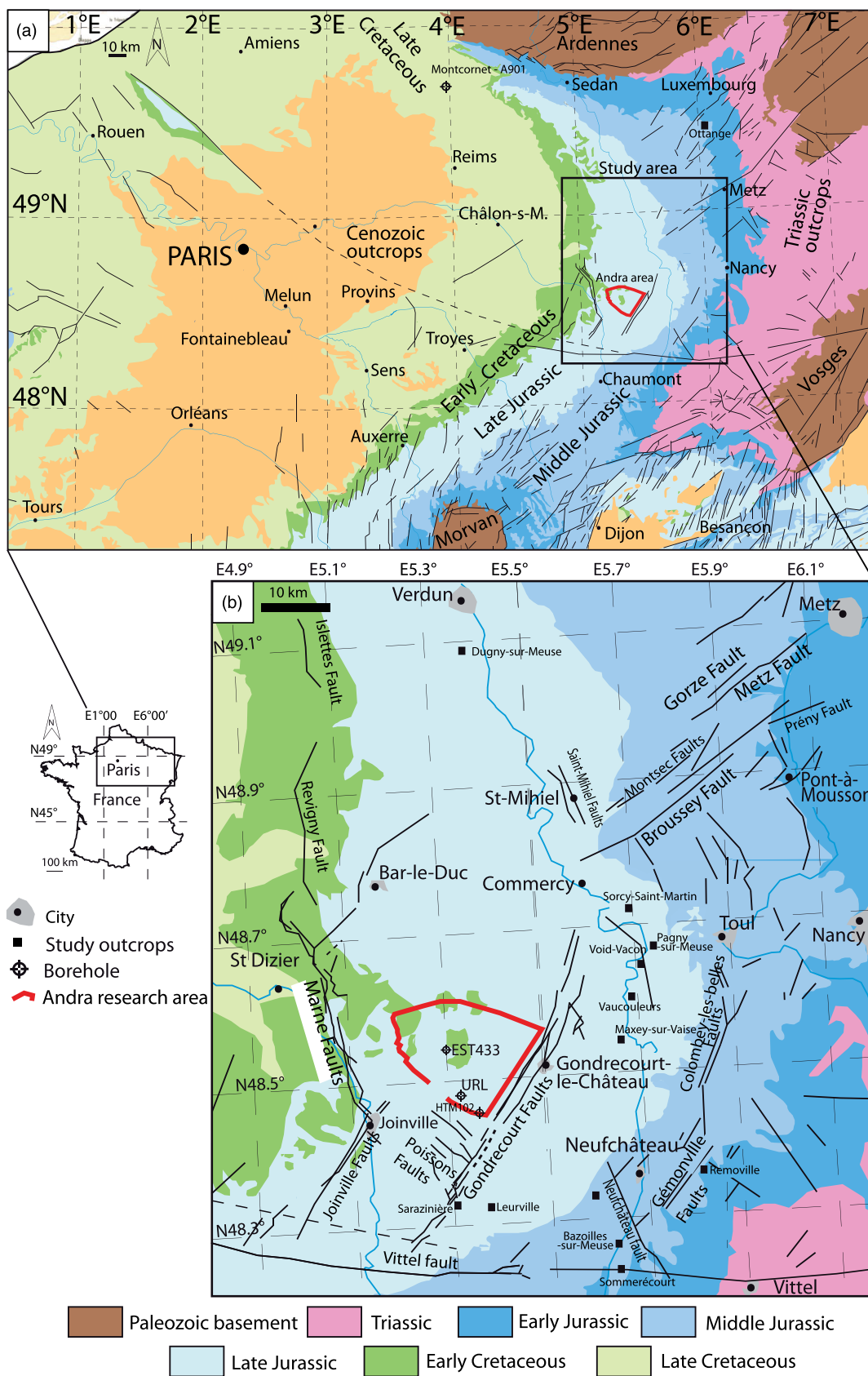


Fig. 1. (a) Geological map of the eastern Paris Basin with (b) a detailed view of the major structures in the studied area. Outcrop and quarry sample locations are indicated by black squares.

At the regional scale, the orientations and relative chronology of minor faults, tension gashes and stylolites can be correlated with the major deformation events recorded in the western European domain during the Meso-Cenozoic period (Bergerat, 1985, 1987; Letouzey, 1986; Villemin, 1986; Coulon & Frizon de Lamotte, 1988; Coulon, 1992; Rocher *et al.* 2004; Bergerat *et al.* 2007; André *et al.* 2010).

While the Triassic was a period of tectonic quiescence, an initial E–W extensional regime is recorded during the Late Triassic period and lasts until Middle Liassic time (Guillocheau *et al.* 2000). A second extension of similar orientation occurred during Late Jurassic time, attributed to the Central Atlantic opening. This regime evolved into an E–W to NE–SW compression during Early Cretaceous time, with two discrete episodes that generated significant uplift and erosion (Guillocheau *et al.* 2000; Brigaud *et al.* 2018): (1) the Late Cimmerian Unconformities corresponding to a succession of two distinct truncations in the Paris Basin and (2) the Late Aptian Unconformity. For some authors however, these Early Cretaceous deformations more likely relate to an extensional regime in the eastern Paris Basin (André *et al.* 2010).

Early Paleocene NNW–SSE to N–S shortening is reported by André *et al.* (2010) in the eastern Paris Basin. Briais *et al.* (2016) showed that long-wavelength deformation occurred in the central Paris Basin during the intra-Maastrichtian to pre-Thanetian period. This deformation, known as the Laramian or Laramide phase (Ziegler, 1990), is well documented in western Europe and is coeval with the North Atlantic opening (Briais *et al.* 2016 and references therein). Briais *et al.* (2016) documented two other deformation phases during the Ypresian period: a minor medium-wavelength deformation during Early Ypresian time that could be a far-field consequence of the North Atlantic rifting, and a long-wavelength deformation during latest Ypresian time, with the emersion of the central Paris Basin in response to the convergence between the Iberian and Eurasian plates. So far, these Ypresian phases are not documented in the eastern border of the Paris Basin.

During Eocene time, the Pyrenean compression generated a NNE–SSW transcurrent regime (Pyr1; André *et al.* 2010) that rotated into NE–SW (Pyr2; André *et al.*, 2010). According to André *et al.* (2010), Pyr2 is strongly expressed in the area, but its age remains uncertain. Indeed, for some authors, a NE–SW compression more likely occurred after the Oligocene extension (Bergerat, 1985).

A NW–SE to E–W extension prevailed during Late Eocene – Oligocene times, and the discontinuities generated during the Pyr1 and Pyr2 strike-slip movements were reactivated as normal and oblique faults (Lacombe *et al.* 1990). The Gondrecourt and Joinville grabens formed at that time, together with the main grabens constituting the ECRIS. Bedding stylolites developed in the Middle and Upper Jurassic carbonates in response to this extensional deformation (Coulon, 1992). Bergerat *et al.* (2007) considered this Oligocene event as the most strongly expressed in the area.

An ENE–WSW shortening, which post-dates the Oligocene extension was recognized by Bergerat (1987) and André *et al.* (2010) and may correspond to a later expression of the Pyrenean compression (Pyr3; André *et al.* 2010).

The Oligocene NW–SE extension switched into a NE–SW extensional regime during the Oligocene–Miocene transition through a σ_2/σ_3 permutation. The Alpine compression is then expressed during Miocene–Pliocene times by a clockwise rotation of σ_1 from WNW–ESE to NNW–SSE (André *et al.* 2010).

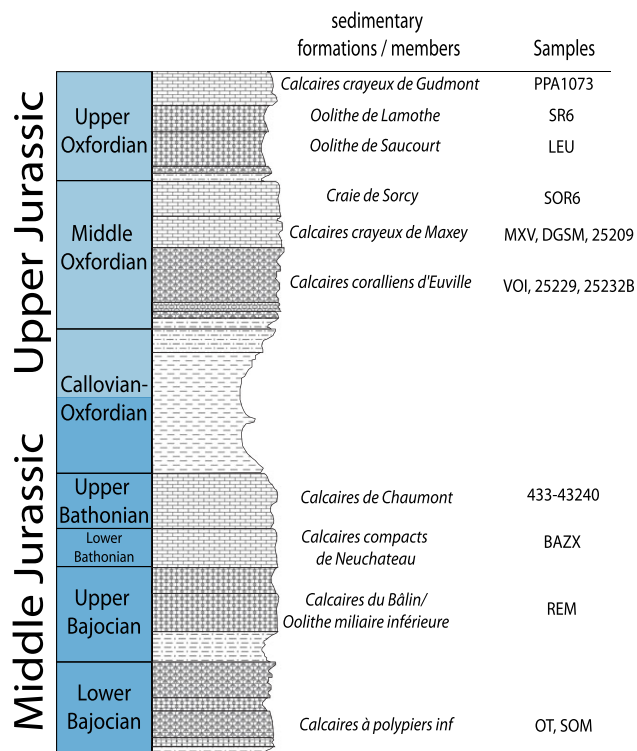


Fig. 2. Simplified lithostratigraphic section in the eastern Paris Basin, showing the position of samples within the stratigraphic formations or members.

It is worth noting that, owing to the lack of a syn-deformation sedimentary record, all age attributions only rely on correlations with the better-constrained tectonic agenda of adjacent domains such as the Rhine Graben, Alpine belt or Pyrenean domain.

3. Material and methods

3.a. Sampling and petrography

Twenty-seven samples were collected from the Middle Jurassic (Bajocian and Bathonian) and Upper Jurassic (Oxfordian) limestones, from outcrops, quarries and boreholes (Fig. 1). They mostly correspond to tension gashes filled by calcite affecting mudstones or grainstones from well-identified sedimentary formations (Fig. 2). The orientation of nine tension gashes is reported. Five samples correspond to calcite filling coral or mouldic vugs, sometimes connected to fractures. Two samples, collected at Leurville (Fig. 1), are hydraulic breccias found as isolated rock fragments dispersed in agricultural crops. Eleven samples contain several tension gashes, either parallel or crossing each other. In three samples, calcite cements filling the intergranular porosity were targeted for U–Pb geochronology.

Samples were either mounted in epoxy or prepared as 30 μm thin-sections and polished. All samples were observed under the optical microscope using transmitted polarized light and under cathodoluminescence (CL) microscopy at 13 keV and 130 mA. For each sample, a series of photomicrographs were gathered to create a composite image (see online Supplementary Material S2).

3.b. Calcite U–Pb geochronology

The method which has been employed is similar to that described in Brigaud *et al.* (2020). Sampling and analysis were performed

using a sector field ICP-MS Element XR (Thermo Scientific™, Waltham, MA, USA) coupled to a 193 nm ArF laser ablation system (TELEDYNE, Thousand Oaks, CA, USA) at the Geosciences Paris-Saclay (GEOPS) laboratory of the University of Paris-Saclay.

Samples and calcite reference materials were ablated at a frequency of 8 Hz and a fluence of 1 to 2 J.cm⁻² with a circular-shaped beam diameter of 150 µm. Glass reference material NIST614 was ablated at a frequency of 10 Hz, a fluence of 6.25 J.cm⁻² and a beam size of 110 µm. Each analysis consisted of 30 s background acquisition followed by 30 s of sample ablation and 30 s washout. Prior to analysis, each spot was pre-ablated during 4 s at a frequency of 8 Hz and with a fluence of 2 J.cm⁻². NIST614 was used to correct for ²⁰⁷Pb/²⁰⁶Pb fractionation, while ²³⁸U/²⁰⁶Pb was corrected using WC-1 (Woodhead *et al.* 2016; Roberts *et al.* 2017). To ensure accuracy, two secondary calcite reference materials were included in each analytical session: Duff Brown Tank (DBT), dated at 64.0 ± 0.7 Ma by U–Pb isotope dilution (Hill *et al.* 2016), and B6, dated at 43.0 ± 1.0 Ma by LA-ICP-MS (Pagel *et al.* 2018). Each analytical sequence is composed of five reference material analyses (one NIST614, one WC-1, one DBT and two B6) inserted at between 10 and 15 spots on unknown calcites. Data were acquired overnight in five sequences of around 400 analyses.

Data were reduced in Iolite® (Paton *et al.* 2011) using the NIST614 glass as the primary reference material for baseline subtraction, to correct for Pb isotope mass bias and for the estimation of ²⁰⁶Pb/²³⁸U and ²⁰⁷Pb/²⁰⁶Pb instrumental drift over the sequencing time. No down-hole fractionation correction is applied in Iolite® (Nuriel *et al.* 2017).

The 2 standard errors in the mean ²⁰⁷Pb/²⁰⁶Pb and ²⁰⁶Pb/²³⁸U ratios measured on NIST614 during the analytical session were propagated to the final age uncertainty of all calcite samples by quadratic addition. Data were plotted on Tera-Wasserburg graphs using IsoplotR online (Vermeesch, 2018), without anchoring the initial ²⁰⁷Pb/²⁰⁶Pb value. Error ellipses of each spot and the error in the Tera-Wasserburg intercept age are at a level of two sigma. In each Tera-Wasserburg graph, a first age uncertainty is given that does not include uncertainty propagations. A second age uncertainty is given, by propagating the systematic uncertainty of the age of primary reference material WC-1 (2.6 %), and the 2 standard errors of the ²⁰⁷Pb/²⁰⁶Pb and ²⁰⁶Pb/²³⁸U of the analytical session by quadratic addition. Sample ages and uncertainties are listed in Table 1 and detailed metadata for LA-ICP-MS calcite U–Pb geochronology are available in the online Supplementary Material.

3.c. Oxygen and carbon stable isotope composition and clumped isotope thermometry

For oxygen and carbon stable isotope analysis, 11 calcite crystals from fracture in-fills were fragmented and collected with tweezers under the magnifying glass. The crystals were subsequently ground into a homogeneous powder in an agate mortar. Oxygen and carbon isotopes were analysed in the Geosciences Laboratory of Rennes University (France) following the methodology described in Malfilatre *et al.* (2012). All isotopic values are reported to the Vienna PeeDee Belemnite (V-PDB) standard (Table 2).

Five samples consisting of large in-fillings were selected for clumped isotope analysis. 30 mg of calcite was sampled using a micro-drilling tool. Δ_{47} measurements were performed at the California Institute of Technology (USA) in two analytical sessions (April and May 2021) with an automated acid digestion and gas purification device coupled to a dual inlet Thermo MAT253, as

described in Passey *et al.* (2010). Samples were weighed into silver capsules (~8 mg) and reacted in a common phosphoric acid bath (~103 %) for 20 minutes at 90 °C under static vacuum. The resulting CO₂ was passed through an ethanol/dry ice U-trap (~–80 °C) before being collected on a liquid nitrogen temperature (–196 °C) U-trap. Following the 20 minutes reaction period, the collected CO₂ was thawed, entrained in helium and carried through a Porapak Q 120/80 mesh gas column held at –20 °C using He as the carrier gas. The purified CO₂ was analysed using a Thermo Scientific MAT 253 mass spectrometer set to collect masses 44–49. Mass 48 was only monitored to detect any hydrocarbon contaminant. $\delta^{18}\text{O}$ and $\delta^{13}\text{C}$ data were also acquired as part of each Δ_{47} analysis and calculated using the parameters reported relative to the PDB reference frame based on the calibrated composition of the laboratory working gas and the correction scheme and constants from Brand *et al.* (2010). In order to account for the temperature dependence of oxygen isotope fractionation between CO₂ gas and carbonate resulting from the reaction with phosphoric acid at 90 °C, a fractionation factor of 1.00811 was used for calcite (following Swart *et al.* 1991). The raw Δ_{47} data were corrected for instrument non-linearity and scale compression (Dennis *et al.* 2011) using several heated (at 1000 °C) and equilibrated gases (at 25 °C) of various bulk isotopic compositions that were run during each session. These gases were used to convert measurements into the inter-laboratory absolute reference frame (Dennis *et al.* 2011). To guarantee accuracy of the Δ_{47} data, we routinely analysed two carbonate reference materials (Carrara marble and TV04). One of these two carbonate standards was analysed once for every five analyses of the unknown samples in order to check for procedural analytical stability and accuracy, and to determine the long-term external reproducibility of our measurements. The Δ_{47} values obtained for these carbonates over the course of this study (May to July 2019) are: $\Delta_{47\text{-CDES25}} = 0.409 \pm 0.016 \text{ ‰}$ (1SD, n = 10) for Carrara; $\Delta_{47\text{-CDES25}} = 0.666 \pm 0.011 \text{ ‰}$ (1SD, n = 8) for TV04, i.e. within accepted Δ_{47} values for TV04 ($\Delta_{47\text{-CDES25}} = 0.655 \text{ ‰}$) and Carrara ($\Delta_{47\text{-CDES25}} = 0.405 \text{ ‰}$). Finally, the corrected Δ_{47} values were converted into temperatures using the composite $\Delta_{47\text{-T}}$ calibration of Bonifacie *et al.* (2017), which has been shown to be appropriate for calcite and dolomite between 0 and 300 °C, and which has been shown to be consistent with measurements made at Caltech. The oxygen isotopic compositions of the water ($\delta^{18}\text{O}_{\text{water}}$) from which the carbonates precipitated were calculated for each estimated $T_{\Delta_{47}}$ using the bulk $\delta^{18}\text{O}_{\text{carb}}$ values and the calcite–water fractionation equation from O’Neil *et al.* (1969).

4. Results

4.a. Calcite petrography

All samples consist of blocky calcite filling tension gashes (Fig. 3) and vugs, apart from the hydraulic breccia sampled at Leurville (LEU samples; Fig. 4). Crystal sizes vary from a few hundred micrometres in small tension gashes to a few millimetres in hydraulic breccias. No syntaxial or antitaxial growth orientations are identified (*sensu* Bons *et al.* 2012). While most samples contain clean crystals, a few of them (e.g. SOM1-1, SOM1-2, REM1) incorporated micrite inclusions from the host rocks during crystallization (Fig. 5). Most samples contain non-luminescent or weakly brown luminescent crystals under CL, without clear successive growth stages. No evidence of multi-phase fracture opening was observed. Apart from samples SOR6-c and DGSM29-1, all fractures are entirely cemented by blocky calcite. No dissolution

Table 1. Samples description and associated calcite U–Pb geochronology data

Samples	Outcrop locality or well	Stratigraphic age	Sedimentary formation or member	Nature	U–Pb age	2 S.E. abs.	2 S.E. %
PPA1073	Andra URL well	Upper Oxfordian	<i>Calcaires crayeux de Gudmont</i>	Tension gash	50.4	2.4	4.7
SR6a	Sarazinière	Upper Oxfordian	<i>Oolithe de Lamothe</i>	Tension gash N50°	58.9	1.8	3.0
SR6b				Tension gash N150°	18.7	1.0	5.6
SR6c				Intergranular cement	57.7	2.6	4.5
LEU1-1	Leurville	Upper Oxfordian	<i>Oolithe de Saucourt</i>	Hydraulic breccia	27.0	1.1	4.2
LEU-2				Hydraulic breccia	22.2	1.2	5.5
A00607c	A901 – Montcornet well	Upper Oxfordian	Unknown	Tension gash	47.3	6.4	13.4
SOR6ab	Sorcy-Saint-Martin	Middle Oxfordian	<i>Craie de Sorcy</i>	Tension gash	47.7	1.7	3.6
SOR6c				Tension gash	44.7	1.6	3.5
MXV7	Maxey-sur-Vaise	Middle Oxfordian	<i>Calcaires crayeux de Maxey</i>	Tension gash N20°	48.0	3.5	7.3
MXV9a				Tension gash N175°	27.4	2.8	10.3
VCLD	Vaucouleurs	Middle Oxfordian	<i>Calcaires crayeux de Maxey</i>	Tension gash N10°	43.2	1.4	3.3
DGSM29-1	Dugny-sur-Meuse	Middle Oxfordian	<i>Calcaires crayeux de Maxey</i>	Tension gash N170°	31.6	2.9	9.2
DGSM29-2a		Middle Oxfordian	<i>Calcaires crayeux de Maxey</i>	Tension gash N170°	32.0	1.5	4.5
DGSM29-2b				Intergranular cement	30.6	7.0	22.8
DGSM7a		Middle Oxfordian	<i>Calcaires crayeux de Maxey</i>	Vug	33.8	2.5	7.4
DGSM7b				Vug	39.0	1.7	4.4
DGSM7c				Tension gash N40°	32.4	7.6	23.5
VOI3b	Void-Vacon	Middle Oxfordian	<i>Calcaires coralliens d'Euville</i>	Tension gash	37.0	1.7	4.7
25209	Andra URL well	Middle Oxfordian	<i>Calcaires crayeux de Maxey</i>	Tension gash	34.9	1.3	3.8
25229	Andra URL well	Middle Oxfordian	<i>Calcaires coralliens d'Euville</i>	Vug	33.2	2.2	6.7
25232B a	Andra URL well	Middle Oxfordian	<i>Calcaires coralliens d'Euville</i>	Tension gash	34.5	2.0	5.9
A901-22a	A901 – Montcornet well	Upper Bathonian	Unknown	Tension gash	92.9	10.3	11.1
A901-22c				Tension gash	68.4	4.0	5.9
A901-22e				Intergranular cement	100.9	22.7	22.5
433-43240	EST433 well	Middle to Upper Bathonian	<i>Calcaires de Chaumont</i>	Tension gash	33.0	5.5	16.6
BAZX90a	Bazoilles-sur-Meuse	Lower Bathonian	<i>Calcaires compacts de Neuchateau</i>	Tension gash N10°	48.5	3.0	6.1
REM3-2	Removille	Upper Bajocian	<i>Calcaire du Bâlin/Oolithe miliaire inf</i>	Tension gash	31.7	3.8	11.9
REM1				Tension gash	42.1	2.7	6.3
OT-1-2	Ottange	Lower Bajocian	<i>Calcaire à polypiers inf</i>	Vug	40.8	2.2	5.4
SOM1-1	Sommerécourt	Lower Bajocian	<i>Calcaire à polypiers inf</i>	Tension gash + vug	42.5	3.9	9.1
SOM1-2				Tension gash + vug	40.9	1.7	4.2

features, such as corrosion gulfs, were observed. Samples SR6 and SOR6 display ambiguous cross-cutting relationships between at least two distinct generations of tension gashes that are filled with

calcite displaying the same cathodoluminescence (Fig. 6). Petrographic illustrations of all samples are available in online Supplementary Material S2.

Table 2. Oxygen and carbon stable isotope composition and clumped isotope thermometry

Samples	Stratigraphic age	Nature	$\delta^{18}\text{O}_{\text{‰V-PDB}}$	$\delta^{13}\text{C}_{\text{‰V-PDB}}$	$\delta^{18}\text{O}_{\text{‰V-PDB}}$ (clumped)	$\delta^{13}\text{C}_{\text{‰V-PDB}}$ (clumped)	T(Δ_{47}) mean (°C)	T(Δ_{47}) error (°C)	$\delta^{18}\text{O}_{\text{‰V-SMOW}}$ water
SR6b	Upper Oxfordian	Tension gash			-7.5	2.7	27	3	-4.6
LEU1-1	Upper Oxfordian	Hydraulic breccia	-10.5	2.8					
LEU-2	Upper Oxfordian	Hydraulic breccia	-8.8	1.7					
SOR6ab	Middle Oxfordian	Tension gash	-7.0	3.2					
VCLD	Middle Oxfordian	Tension gash	-7.7	3.4	-7.8	3.3	37	2	-2.9
VOI3b	Middle Oxfordian	Tension gash	-7.1	3.1					
25209	Middle Oxfordian	Tension gash	-8.4	2.9	-8.6	2.9	41	1	-2.9
25229	Middle Oxfordian	Vug	-9.0	2.9	-8.9	2.7	42	2	-3.1
A901-22a	Upper Bathonian	Tension gash	-7.9	1.1					
BAZX90a	Lower Bathonian	Tension gash	-10.5	1.4	-10.3	1.4	53	5	-2.6
REM1	Upper Bajocian	Tension gash	-10.3	1.5					
SOM1-1	Lower Bajocian	Tension gash + vug	-9.1	2.0					

4.b. U–Pb ages

Among the 27 samples collected for the purpose of this study, four were not amenable to U–Pb geochronology and were thus excluded. A total of 32 U–Pb ages are reported (Table 1). The oldest age measured in tension gashes is found in the Upper Bathonian sampled in the Montcornet borehole (sample A901-22), dated at 92.9 ± 10.3 Ma. In the same sample, another population of tension gashes is dated at 68.4 ± 4.0 Ma. In the Sarazinière quarry, a tension gash oriented N50° (sample SR6a) gives an age of 58.9 ± 1.8 Ma. Most of the ages obtained are between 50.4 ± 2.4 Ma (sample PPA1073) and 27.4 ± 2.8 Ma (sample MXV9a). A hydraulic breccia sampled at Leurville (sample LEU-2) gives an age of 22.2 ± 1.2 Ma. Finally, a tension gash oriented N150° gives a younger age of 18.7 ± 1.0 Ma (sample SR6b).

In addition, three ages were measured in the intergranular calcite cements, yielding ages of 100.9 ± 22.7 Ma (sample A901-22e), 57.7 ± 2.6 Ma (sample SR6c) and 30.6 ± 7.0 Ma (sample DGSM29-2b).

4.c. Oxygen and carbon stable isotope composition and clumped isotopes

$\delta^{18}\text{O}$ values range between -7.0 ‰_{V-PDB} (sample SOR6ab) and -10.5 ‰_{V-PDB} (samples BAZX90a and LEU1-1), while $\delta^{13}\text{C}$ are between 1.1 ‰_{V-PDB} (sample A901-22a) and 3.4 ‰_{V-PDB} (sample VCLD). $\delta^{18}\text{O}$ and $\delta^{13}\text{C}$ values measured by clumped isotopy are identical within the limits of analytical uncertainty to the ones obtained from the traditional method where C and O stable isotope compositions are measured separately. The highest Δ_{47} temperature is obtained for sample BAZX90a (53 ± 5 °C), and the lowest

for sample SR6b (27 ± 3 °C). Three other samples give temperatures of 37 ± 2 °C (VCLD), 41 ± 1 °C (25209) and 42 ± 2 °C (25229). Sample types and associated isotopic values are summarized in Table 2.

5. Discussion

5.a. Ages, impact and duration of brittle deformation

Since no syntaxial or antitaxial growth orientations were identified (*sensu* Bons *et al.* 2012), the syn-kinematic precipitation of calcite crystals within tension gashes is unclear (Roberts & Holdsworth, 2022). Field observations have revealed that tension gashes are generally associated with tectonic stylolites, suggesting syn-kinematic calcite dissolution and recrystallization (André *et al.* 2010). Furthermore, although CL sectorial zoning is observed in some samples, no successive calcite growth stages can be clearly determined, suggesting that all crystals filling a given tension gash or vug are monogenic. An isochron obtained from the sampling of several crystals filling a given tension gash proves that calcite formed during a single precipitation event. Yet, calcite cements can post-date fracture opening. Such uncertainty is somehow minimized by the large number of samples considered for this research, and by the good agreement between the orientation of fractures and their U–Pb ages, which will be discussed below.

Calcite mechanical twinning is observed in some samples (LEU1-1, VCLD, BAZX90a, REM-3-2, REM1, OT-1-2, SOM1-1, SOM1-2). The development of such twinning cannot be correlated with the age or location of the samples. The absence of calcite twinning in most samples may be due to the small size of blocky calcite crystals filling tension gashes (Lacombe *et al.* 1990).

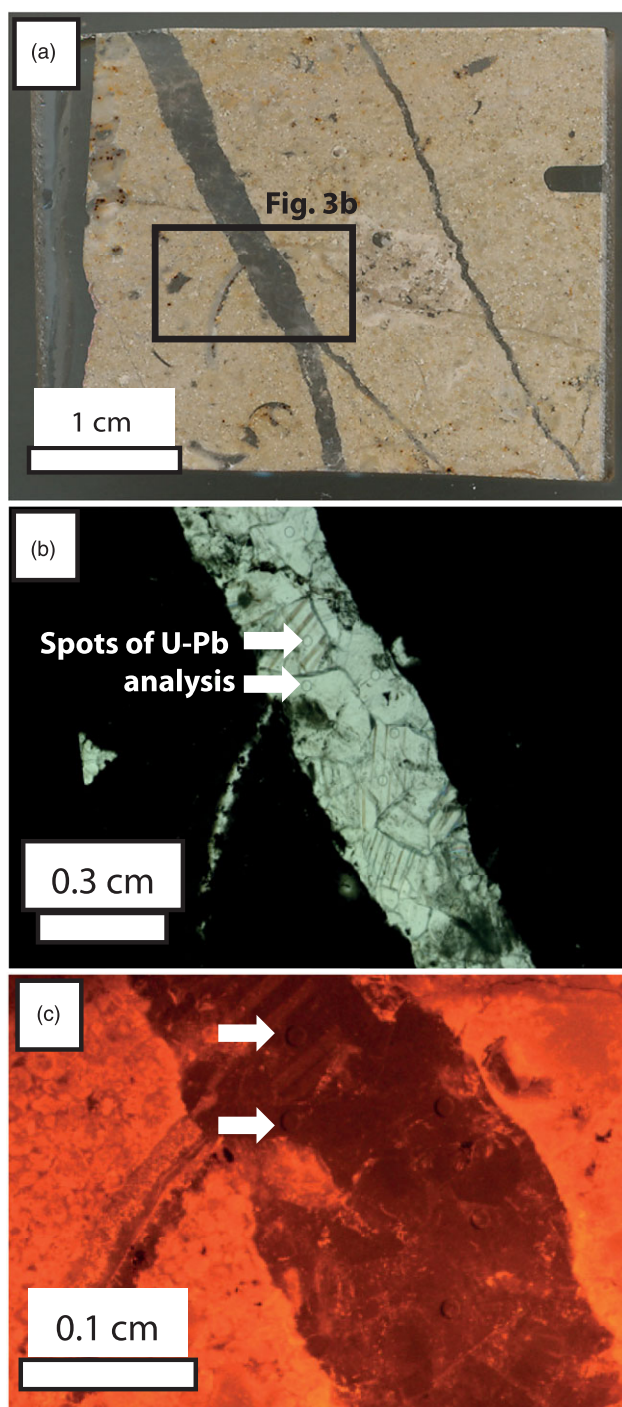


Fig. 3. (a) Example of sub-parallel tension gashes affecting a wackestone sampled at Bazoilles-sur-Meuse (sample BAZX90a) in (b) transmitted light and (c) cathodoluminescence microscopy. Ablation craters (150 μm in diameter) are visible in (b) and (c) (white arrows).

The tension gash showing the oldest age was sampled in the Montcornet borehole, located ~ 200 km northwest of the Andra URL, in the vicinity of the Ardennes massif (Fig. 1). The U–Pb age of 92.9 ± 10.3 Ma suggests the Albian to Santonian period, which may be related to a major inversion phase documented in northern France (Bergerat & Vandycke, 1994). Interestingly, this calcite U–Pb age matches with the age obtained on the first dolomite cement identified in the Middle Jurassic at depth in the central

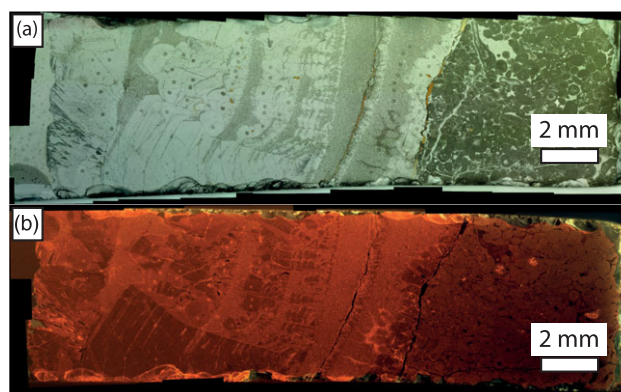


Fig. 4. Hydraulic breccia developed in the *Oolithe de Saucourt* Formation (sample LEU-2) in (a) transmitted light and (b) cathodoluminescence microscopy. Ablation craters (150 μm in diameter) are visible.

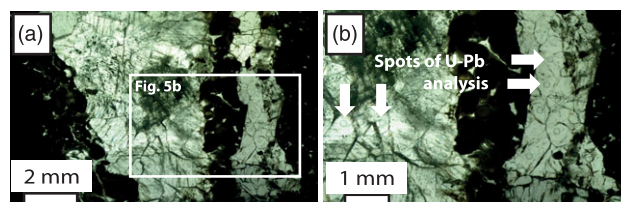


Fig. 5. Tension gash in the *Oolithe miliaire* Formation sampled at Removille (sample REM1) observed in transmitted light. The white square in photomicrograph (a) corresponds to the magnification in (b). This sample illustrates the impurities contained in some calcite cements. Ablation craters (150 μm in diameter) are visible (white arrows) and located, when possible, in the most limpid parts of the crystals.

Paris Basin (Mangenot *et al.* 2018). Our data agree with André *et al.* (2010) and tends to indicate the absence of this tectonic phase around the Andra URL. Another sample in the same borehole was dated at 68.4 ± 4.0 Ma, i.e. the Cretaceous–Paleocene transition (Fig. 7). This age cannot be confidently interpreted and attributed to a known deformation phase. It may either be linked to the so-called ‘sub-Hercynian’ inversion phase defined by Ziegler (1987) or to an early stage of the Pyrenean compression, as evidenced in the southeastern Pyrenees (Cruset *et al.* 2020). In the central Paris Basin, a second blocky calcite generation was also dated at 68.5 ± 7.7 Ma in the deep Middle Jurassic (Mangenot *et al.* 2018). Regardless, these early phases recorded here more than 150 km north or west of the URL are not described in the eastern Paris Basin, where brittle structures are mostly thought to be Cenozoic in age (Bergerat *et al.* 2007; André *et al.* 2010; this study). Indeed, the ages of tension gashes and hydraulic breccias documented here span from 58.9 ± 1.8 Ma to 18.7 ± 1.0 Ma, i.e. from the Thanetian to the Burdigalian periods (Fig. 7).

Our data show that tectonic quiescence then prevailed during Paleocene and Early Ypresian times, a result in agreement with the slow rate of N–S convergence between the Iberian and Eurasian plates during this period (Macchiavelli *et al.* 2017; Grool *et al.* 2018; Mouthereau *et al.* 2021). A single tension gash oriented N50° is dated at 58.9 ± 1.8 Ma (Paleocene) in the Sarazinière quarry. This fracture may be related to an early stage of the Pyrenean compression. Alternatively, this event may be linked to the so-called ‘Laramide’ phase (Ziegler, 1987), which corresponds to a major inversion period with an uplift and erosion quantified to ~ 600 m in the Morvan Massif, south of the Paris

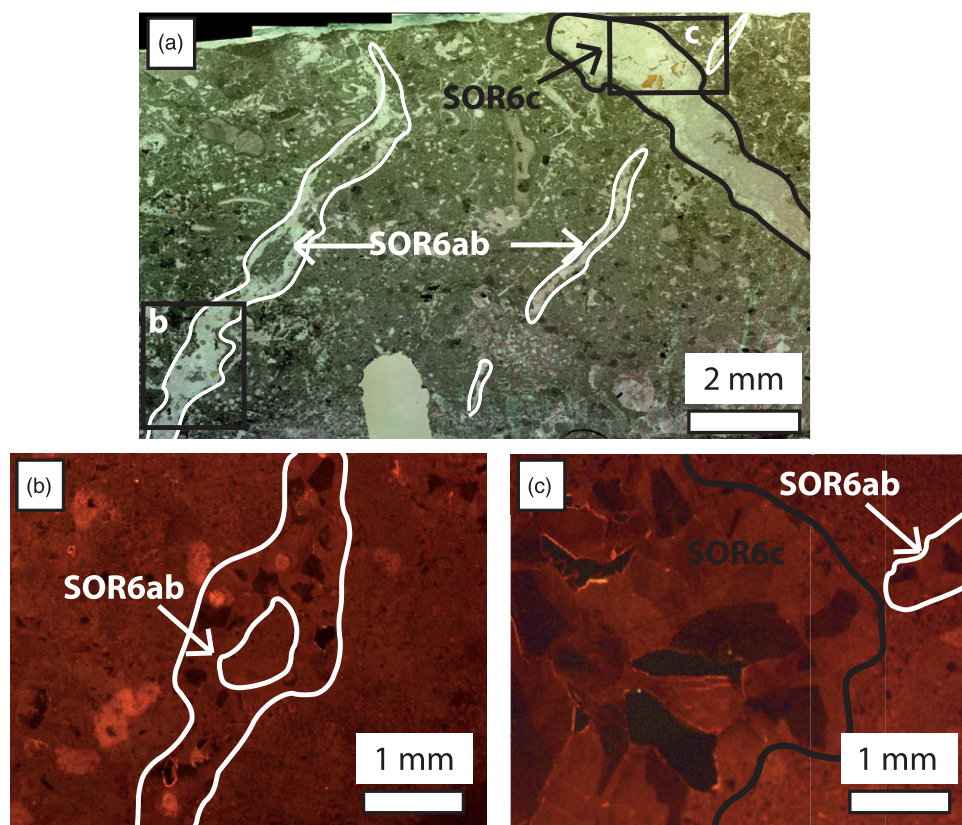


Fig. 6. Tension gashes developed in sample SOR6 (Sorcy-Saint-Martin locality). The relative chronology between the fractures encircled in white (SOR6ab) and in black (SOR6c) is unclear, because no clear cross-cutting relationship is visible. Moreover, both tension gash populations are filled by blocky calcite displaying comparable cathodoluminescence.

Basin, and to 300 m in the study area (Barbarand *et al.* 2013; Blaise *et al.* 2014). This event does not seem to be restricted to the eastern border of the Paris Basin, since a U–Pb age of 61.1 ± 2.5 Ma was documented for calcite cements in the Middle Jurassic at depth in the central Paris Basin (Mangenot *et al.* 2018).

A continuous deformation is then recorded in the age distribution of tension gashes from the Late Ypresian to the Rupelian, although two age clusters can be evidenced between 40–50 Ma (nine samples) and 30–35 Ma (seven samples) (Fig. 7). The first age cluster (40–50 Ma) is associated with N10° to N20° tension gashes (BAZX90a, MXV7, VCLD). The Late Ypresian to Bartonian opening and filling of these gashes probably records the far-field onset of the main Pyrenean compressional event at that time (Macchiavelli *et al.* 2017). Within this deformation phase, discrete tectonic pulses may have generated higher rates of fracturing. A cluster of ages is recorded at *c.* 48 Ma (samples A00607c, SOR6ab, SOR6c, BAZX90a), synchronous with the emersion of the central Paris Basin (Briais *et al.* 2016) in response to the main Pyrenean compression period (e.g. Cruset *et al.* 2020). Several tension gashes are then dated at *c.* 43 Ma (Fig. 7), matching the U–Pb ages reported by Pagel *et al.* (2018) along the Gondrecourt graben and the age of a vertical tension gash in HTM102 borehole close to the Andra URL (Brigaud *et al.* 2020).

A reactivation of the Variscan Vittel fault south of the studied area is evidenced by two fractures sampled in the Sommerécourt quarry and dated at 42.5 ± 3.9 Ma and 40.9 ± 1.7 Ma (Fig. 7). At Removille, sample REM1 was collected along a fault delimiting a small graben of similar orientation to the Gondrecourt and Joinville grabens. The age of this sample, 42.1 ± 2.7 Ma confirms the synchronous formation of these structures. Finally, sample OT1-2 from the Ottange quarry dated at 40.8 ± 2.2 Ma demonstrates that this intraplate deformation extended far north of the

study area (Fig. 1). They are also recorded in the central Paris Basin, as documented by Mangenot *et al.* (2018). These deformations and cementations are all interpreted as a far-field consequence of Pyrenean shortening.

A few fractures are dated between 40 and 35 Ma, while another main fracturing event is identified at *c.* 33 Ma (Fig. 7; Table 1). Ten of the 32 measured U–Pb ages obtained are in the 35–30 Ma range, matching previous U–Pb ages of *c.* 33 Ma reported for fractures along the Gondrecourt faults (Pagel *et al.* 2018) and vug-filling calcites in Oxfordian limestones from the Andra URL borehole cores (Pisapia *et al.* 2018). Following Pagel *et al.* (2018) by analogy with the known tectonic agenda of the Rhine Graben, we suggest that these dated structures are related to extensional deformation and the opening of the ECRIS (Dèzes *et al.* 2004; Bergerat *et al.* 2007; Ring & Gerdes, 2016), an event that is strongly expressed in the eastern Paris Basin (Bergerat *et al.* 2007) as attested to by the formation of the small Gondrecourt and Joinville grabens. A second generation of tension gashes collected along the Removille graben (REM3-2) yield an age of 31.7 ± 3.8 Ma, showing that this graben was formed through a two-step evolution identical to the Gondrecourt graben, i.e. a strike-slip or oblique displacement during Lutetian time, followed by extension during Rupelian time.

On the other hand, we cannot fully exclude a compressional origin for all of these *c.* 33 Ma tension gashes as a consequence of further Pyrenean or Alpine far-field deformations (Cruset *et al.* 2020; Parizot *et al.* 2021). Regardless, we show here that deformation in the eastern Paris Basin occurred continuously from Late Ypresian to Rupelian times (Fig. 7) and that the transition from a contractional regime prevailing during the Eocene period to an extensional deformation during Oligocene time may have been progressive.



Fig. 7. Compilation of calcite U–Pb ages in tension gashes and hydraulic breccias. In the histogram, data are plotted without considering the corresponding age uncertainties.

After this 33 Ma ECRIS-related event, few younger gashes are dated at *c.* 30 Ma. Tension gashes developed in the quarries of Dugny-sur-Meuse and Maxey-sur-Vaise dated at *c.* 32–27 Ma are oriented N170° and N175° and may have opened during a compressional phase documented by Bergerat (1987) and André et al. (2010) and interpreted as a late Pyrenean horizontal stress. This age also replicates the ones obtained by Parizot et al. (2021) in the north Pyrenean foreland basin, and those of Cruset et al. (2020) in the southern Pyrenees, interpreted as a short-lived reactivation of the compression at that time and whose expression is recorded up to the southern coast of England (Parrish et al. 2018). Alternatively, such tension gashes could have formed in response to a NE–SW extension generated from an interchange between σ_2 and σ_3 (André et al. 2010).

Post-Rupelian brittle structures are scarce (Fig. 7). The absence of tension gashes dated between *c.* 27 Ma and 22 Ma suggests a period of quiescence during Chattian time before the renewal of compressive deformation. Calcite-cemented hydraulic breccias affecting the *Oolithe de Saucourt* Formation precipitated during the Chattian–Aquitanian period. In the Sarazinière quarry, a tension gash oriented N150° gave a younger age of 18.7 ± 1.0 Ma. Thus, this renewal of deformation had a limited impact on the opening of fractures in the eastern Paris Basin. This is in agreement with field observations that documented poorly developed tectonic microstructures related to the Miocene period (André et al. 2010), and the absence of reactivation of the main discontinuities (Bergerat et al. 2007).

Both Miocene calcites were sampled in the vicinity of the NW–SE Poissons fault system (Fig. 1) that reactivated in response to the compression during either the earliest stages of the Alpine contractional stress or a late Pyrenean event during Aquitanian/Burdigalian times (Hoareau et al. 2021; Parizot et al. 2021).

Finally, the absence of younger ages indicates that the growth of the nearby Jura fold-and-thrust belt formed roughly between 11 and 3 Ma (Homberg et al. 2002; Smeraglia et al. 2021) had no or very limited impact on the deformation of the eastern Paris Basin.

To sum up, the deformation of the eastern Paris Basin is essentially related to far-field propagation of compressional stress during the Pyrenean orogen growth. It has been accommodated continuously by the opening of tension gashes and the development or reactivation of strike-slip faults and stylolites between *c.* 50 Ma (sample PPA1073) and 27 Ma (sample MXV9a), with deformation pulses at *c.* 48 Ma and 43 Ma, and only interrupted for a short time by the ECRIS-related extensional event at *c.* 33 Ma.

On a larger scale, this tectonic agenda of the eastern Paris Basin is consistent with the U–Pb ages of slickenfibres and fracture-fill calcites in the north foreland basin of the Pyrenees (Parizot et al. 2021), in the southeastern Pyrenean fold-and-thrust belt and the south foreland Ebro basin (Cruset et al. 2020) and along the Cevennes fault system (Parizot et al. 2022). South of the Paris Basin, fluorite mineralization occurred likely in response of this contractional event (Lenoir et al. 2021). This event is also recorded in the Jura fold-and-thrust belt, where a pre-orogenic NE–SW strike-slip fault was recently evidenced through U–Pb geochronology of slickenfibres yielding two ages similar to ours at 48.4 ± 1.5 Ma and 44.7 ± 2.6 Ma (Smeraglia et al. 2021).

5.b. Origin and temperature of calcite-mineralizing fluids

The meteoric origin of waters from which calcite precipitated in tension gashes was suggested by André et al. (2010) on the basis

of the $\delta^{18}\text{O}$ values measured in calcite. Yet, the oxygen stable isotope composition of parent-waters was uncertain, since the fractionation factor between H_2O and calcite was estimated from only six two-phased aqueous fluid inclusions that homogenized at temperatures ranging from 31 to 38 °C (Buschaert *et al.* 2004). Thanks to the Δ_{47} clumped isotope composition of calcite, the origin of parent-waters can be determined with a higher level of confidence, especially in low-temperature environments in which aqueous inclusions remain in a single-phase metastable state (Goldstein & Reynolds, 1994). The $\delta^{18}\text{O}$ values of calcite-mineralizing waters, determined on five samples from their clumped isotope composition, range from -4.6 to -2.6 ‰ $_{\text{V-SMOW}}$, supporting the views of André *et al.* (2010) and Pagel *et al.* (2018) regarding their meteoric origin.

The temperature at which calcite cements precipitated in veins and hydraulic breccias along the Gondrecourt graben was lower than 50 °C (Pagel *et al.* 2018), slightly higher than the expected temperature of the host rock. Yet, Brigaud *et al.* (2020) reported higher temperatures, up to 90 °C, in a calcite-filled tension gash dated at 41.5 ± 4.8 Ma at the vicinity of the Gondrecourt graben (well HTM102 located 2 km from the graben; Fig. 7). These temperatures suggest that hot fluid flow migrated along deeply rooted faults during the Ypresian/Bartonian compressional regime (Brigaud *et al.* 2020). Here, the highest Δ_{47} temperature is c. 53 °C in the *Calcaires de Chaumont* Formation (Bathonian), showing that meteoric waters were slightly in thermal disequilibrium with their host rocks. In such case, meteoric waters from deeper strata may have risen upward through the fracture network (Ge & Garven, 1992; Sibson, 1994). In addition, the Δ_{47} temperatures may also reflect the burial depth at which calcite precipitation occurred: the oldest fractures may have developed at a depth of 700 to 1000 m. Since the eastern Paris Basin experienced inversion and associated erosion during Cenozoic times, the youngest fractures (Miocene) were generated closer to the present-day surface (Fig. 8).

5.c. Origin of intergranular calcite cements

The impact of Cenozoic intraplate deformation in the interparticle cementation of the Jurassic limestones in the eastern Paris Basin is still unclear. André *et al.* (2010) and Carpentier *et al.* (2014) stressed that contractional deformation generated vertical stylolites with horizontal peaks and that a high density of bed-parallel stylolites could be attributed to the Late Eocene – Oligocene extensional period. These tectonic stylolites developed during the inversion of the eastern Paris Basin and may have contributed to calcite dissolution–recrystallization and eventually to the cementation of intergranular pores (Buschaert *et al.* 2004; André *et al.* 2010). This scenario is supported by recent U–Pb ages of vug-filling calcite in the Oxfordian limestones at c. 33 Ma (Pisapia *et al.* 2018), showing that the Late Eocene – Oligocene extension effectively contributed to occlude the pore space.

Among the samples considered for this research, three display blocky calcite cementing the intergranular porosity large enough to be targeted for U–Pb dating. In sample DGSM29-2, these blocky calcites yielded an age of 30.6 ± 7.0 Ma (DGSM29-2b; Table 1), identical, within the limits of analytical uncertainties, to the age of the nearby N170° tension gashes (DGSM29-2a and DGSM29-1) at 32.0 ± 1.5 Ma and 31.6 ± 2.9 Ma. In sample A901-22, blocky calcite cements filling intergranular pores are dated at 100.9 ± 22.7 Ma (A901-22e), matching the age of the nearby fracture dated at 92.9 ± 10.3 Ma (A901-22a). However,

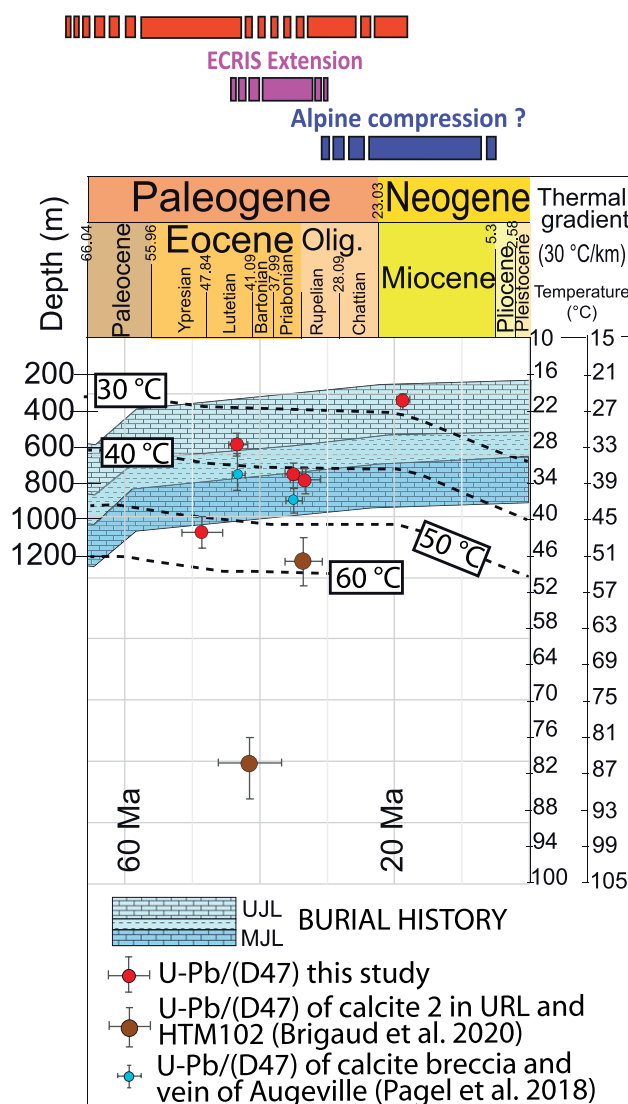


Fig. 8. Calcite U–Pb age as a function of crystallization temperature determined from Δ_{47} thermometry.

age uncertainties are large for this sample, which may be explained by low U/Pb ratios together with the presence of a younger calcite infilling fractures (A901-22c, dated at 68.4 ± 4 Ma), which may have induced the dissolution–recrystallization of the older calcite cement. A third example is illustrated in Figure 9 with a grainstone sampled at the Sarazinière quarry (*Oolithe de Lamothe* Formation, Upper Oxfordian), affected by two generations of tension gashes. The first generation is oriented N50° and yields an age of 58.9 ± 1.8 Ma (SR6a), while the second is oriented N150° and is dated at 18.7 ± 1.1 Ma (SR6b). Both tension gashes are filled by calcite crystals displaying the same cathodoluminescence (Fig. 9), hence the difficulty in establishing a relative chronology from their cross-cutting relationship. Calcite U–Pb geochronology resolves this issue. Moreover, the intergranular pore space is entirely plugged by a blocky calcite showing a comparable dull brown cathodoluminescence. The U–Pb age of this blocky calcite, 57.7 ± 2.6 Ma (SR6c), is identical to the older tension gash (SR6a, 58.9 ± 1.8 Ma). It is worth noting that these ages match the one obtained on the second blocky

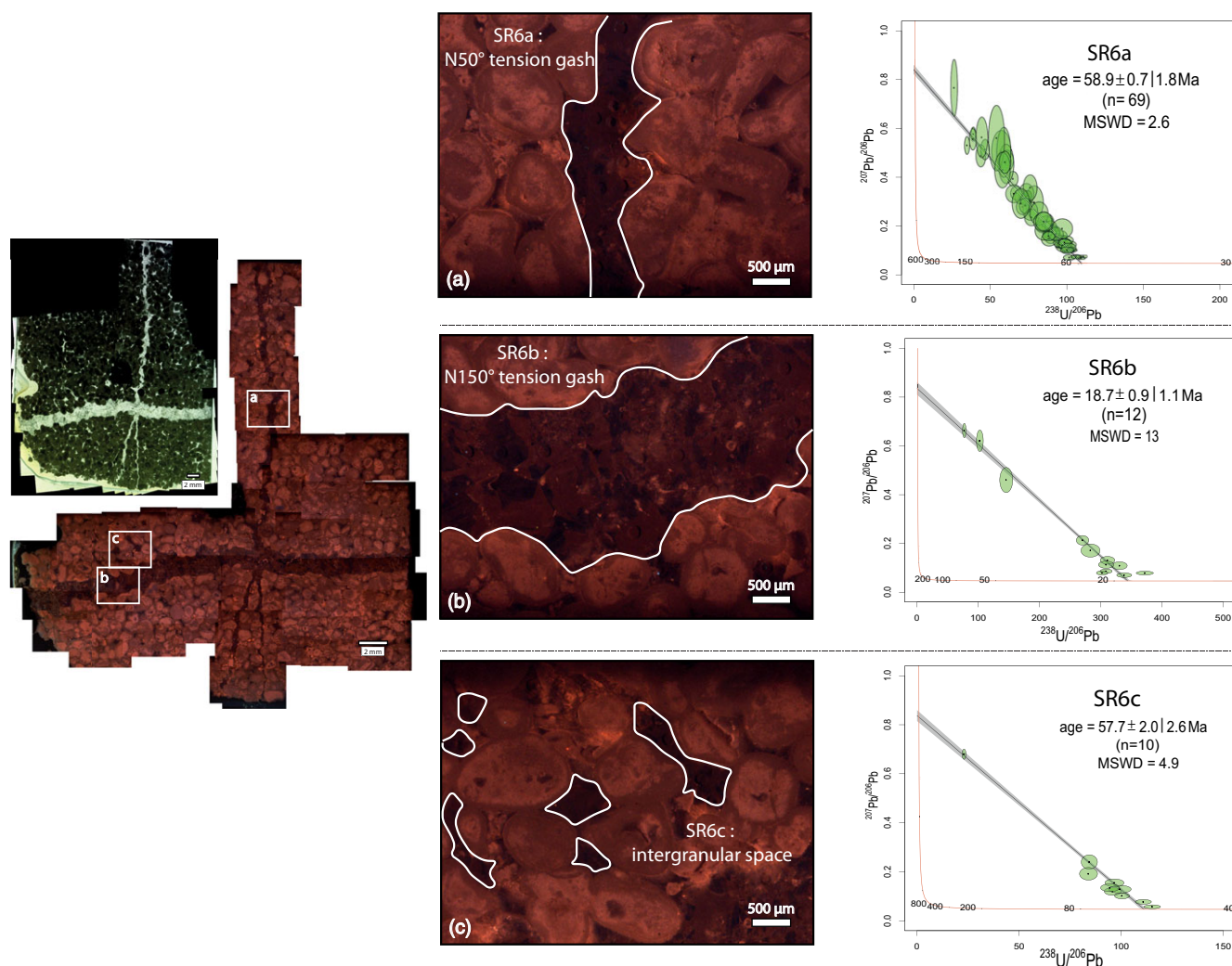


Fig. 9. Calcite U–Pb ages determined in the SR6 sample (Sarazinière quarry, *Oolithe de Lamothe* Formation, Upper Oxfordian).

calcite generation in the deep Middle Jurassic carbonate strata from the Paris Basin depocentre (Mangenot *et al.* 2018).

Therefore, although tension gashes could have acted as preferential conduits for meteoric waters, fluid flow and associated calcite crystallization were not only restricted to the fracture network. Palaeo-water flows through the intergranular porosity and subsequent cementation was enhanced by the development of brittle microstructures (Hansman *et al.* 2018; Sun *et al.* 2022). This is shown by the synchronous precipitation of calcite in tension gashes and in the adjacent intergranular pore space. However, the spatial extension of such ‘tectonic-induced cementation’ is unknown and needs further research and complementary geochronological data on calcite cements occluding the intergranular pore space.

6. Conclusions

We have provided evidence for a continuous fracturing of the Jurassic carbonates from the Ypresian to the Rupelian period in the eastern Paris Basin. This period coincides with the main shortening related to the Pyrenean orogen growth, interrupted by extensional deformation during Late Eocene – Early Oligocene times. Three U–Pb age clusters are identified, the first two at *c.* 48 Ma and 43 Ma, related to the far-field propagation of Pyrenean

horizontal stress, and a third at 33 Ma corresponding to the ECRIS-related extensional regime. Fluids of meteoric origin percolated through the fracture networks at rather low temperatures (from 27 to 53 °C), with a progressive decrease of temperature though time. Fluid flow and associated calcite precipitation was not restricted within the fractures, but also occurred in the intergranular pore space.

Supplementary material. To view supplementary material for this article, please visit <https://doi.org/10.1017/S0016756822000772>

Acknowledgements. This manuscript benefited from fruitful discussion with Christian Hibsich. We also thank Frédéric Haurine for his assistance during the LA-ICP-MS U–Pb analysis. This work is the outcome of a collaborative project between the University Paris-Saclay and Andra, the French agency for radioactive waste management, funded in part by Andra. We thank the two anonymous reviewers for their constructive comments that helped to improve the manuscript.

Conflict of interest. None.

References

André G, Hibsich C, Fourcade S, Cathelineau M and Buschaert S (2010) Chronology of fracture sealing under a meteoric fluid environment:

- microtectonic and isotopic evidence of major Cainozoic events in the eastern Paris Basin (France). *Tectonophysics* **490**, 214–28.
- Barbarand J, Quesnel F and Pagel M** (2013) Lower Paleogene denudation of Upper Cretaceous cover of the Morvan Massif and southeastern Paris Basin (France) revealed by AFT thermochronology and constrained by stratigraphy and paleosurfaces. *Tectonophysics* **608**, 1310–27.
- Beaudoin N, Lacombe O, Roberts NMW and Koehn D** (2018) U–Pb dating of calcite veins reveals complex stress evolution and thrust sequence in the Bighorn Basin, Wyoming, USA. *Geology* **46**, 1015–8.
- Bergerat F** (1985) *Déformations cassantes et champs de contrainte tertiaires dans la plate-forme européenne*. Ph.D. thesis, Université Pierre et Marie Curie – Paris VI, Paris, France. Published thesis.
- Bergerat F** (1987) Stress fields in the European platform at the time of Africa–Eurasia collision. *Tectonics* **6**, 99–132.
- Bergerat F, Elion P, Frizon de Lamotte D, Proudhon B, Combes P, André G, Willeveau Y, Laurent-Charvet S, Kouradian R, Lerouge G and Ott d'Estevou P** (2007) 3D multiscale structural analysis of the Eastern Paris Basin: the ANDRA contribution. *Mémoire de la Société géologique de France* **178**, 15–35.
- Bergerat F and Vandycke S** (1994) Palaeostress analysis and geodynamical implications of Cretaceous–Tertiary faulting in Kent and the Boulonnais. *Journal of the Geological Society, London* **151**, 439–48.
- Blaise T, Barbarand J, Kars M, Ploquin F, Aubourg C, Brigaud B, Cathelineau M, El Albani A, Gautheron C, Izart A, Janots D, Michels R, Pagel M, Pozzi J-P, Boiron M-C and Landrein P** (2014) Reconstruction of low temperature (<100 °C) burial in sedimentary basins: a comparison of geothermometer in the intracontinental Paris Basin. *Marine and Petroleum Geology* **53**, 71–87.
- Blaise T, Cathelineau M, Boulvais P, Techer I, Boiron M-C, Tarantola A, Brigaud B and Landrein P** (2022) Origin of ⁸⁷Sr enrichment in calcite cements in Jurassic limestones (Eastern Paris Basin, France). *Applied Geochemistry* **136**, 105–31.
- Bonifacie M, Calmels D, Eiler JM, Horita J, Chaduteau C, Vasconcelos C, Agrinier P, Katz A, Passey BH, Ferry JM and Bourrand J-J** (2017) Calibration of the dolomite clumped isotope thermometer from 25 to 350 °C, and implications for a universal calibration for all (Ca, Mg, Fe) CO₃ carbonates. *Geochimica et Cosmochimica Acta* **200**, 255–79.
- Bons PD, Elburg MA and Gomez-Rivas E** (2012) A review of the formation of tectonic veins and their microstructures. *Journal of Structural Geology* **43**, 33–62.
- Brand WA, Assonov SS and Coplen TB** (2010) Correction for the ¹⁷O interference in δ(¹³C) measurements when analyzing CO₂ with stable isotope mass spectrometry (IUPAC Technical Report). *Pure and Applied Chemistry* **82**, 1719–33.
- Briaux J, Guillocheau F, Lasseur E, Robin C, Châteauneuf JJ and Serrano O** (2016) Response of a low-subsiding intracratonic basin to long wavelength deformations: the Palaeocene–early Eocene period in the Paris Basin. *Solid Earth* **7**, 205–28.
- Brigaud B, Bonifacie M, Pagel M, Blaise T, Calmels D, Haurine F and Landrein P** (2020) Past hot fluid flows in limestones detected by Δ₄₇–(U–Pb) and not recorded by other geothermometers. *Geology* **48**, 851–6.
- Brigaud B, Durllet C, Deconinck J-F, Vincent B, Pucéat E, Thierry J and Trouiller A** (2009) Facies and climate/environmental changes recorded on a carbonate ramp: a sedimentological and geochemical approach on Middle Jurassic carbonates (Paris Basin, France). *Sedimentary Geology* **222**, 181–206.
- Brigaud B, Pucéat E, Pellenard P, Vincent B and Joachimski MM** (2008) Climatic fluctuations and seasonality during the Late Jurassic (Oxfordian–Early Kimmeridgian) inferred from δ¹⁸O of Paris Basin oyster shells. *Earth and Planetary Science Letters* **273**, 58–67.
- Brigaud B, Vincent B, Carpentier C, Robin C, Guillocheau F, Yven B and Huret E** (2014) Growth and demise of the Jurassic carbonate platform in the intracratonic Paris Basin (France): interplay of climate change, eustasy and tectonics. *Marine and Petroleum Geology* **53**, 3–29.
- Brigaud B, Vincent B, Pagel M, Gras A, Noret A, Landrein P and Huret E** (2018) Sedimentary architecture, depositional facies and diagenetic response to intracratonic deformation and climate change inferred from outcrops for a pivotal period (Jurassic/Cretaceous boundary, Paris Basin, France). *Sedimentary Geology* **373**, 48–76.
- Bruna P-O, Guglielmi Y, Lamarche J, Floquet M, Fournier F, Sizun J-P, Gallois A, Marié L, Bertrand C and Hollender F** (2013) Porosity gain and loss in unconventional reservoirs: example of rock typing in Lower Cretaceous hemipelagic limestones, SE France (Provence). *Marine and Petroleum Geology* **48**, 186–205.
- Buschaert S, Fourcade S, Cathelineau M, Deloule E, Martineau F, Ayt Ougougdal M and Trouiller A** (2004) Widespread cementation induced by inflow of continental water in the eastern part of the Paris basin: O and C isotopic study of carbonate cements. *Applied Geochemistry* **19**, 1201–15.
- Carpentier C, Brigaud B, Blaise T, Vincent B, Durllet C, Boulvais P, Pagel M, Hibsche C, Yven B, Lach P, Cathelineau M, Boiron M-C, Landrein P and Buschaert S** (2014) Impact of basin burial and exhumation on Jurassic carbonates diagenesis on both sides of a thick clay barrier (Paris Basin, NE France). *Marine and Petroleum Geology* **53**, 44–70.
- Carpentier C, Lathuilière B and Ferry S** (2010) Sequential and climatic framework of the growth and demise of a carbonate platform: implications for the peritidal cycles (Late Jurassic, North-eastern France): growth and demise of a carbonate platform. *Sedimentology* **57**, 985–1020.
- Carpentier C, Lathuilière B, Ferry S and Sausse J** (2007) Sequence stratigraphy and tectonosedimentary history of the Upper Jurassic of the Eastern Paris Basin (Lower and Middle Oxfordian, Northeastern France). *Sedimentary Geology* **197**, 235–66.
- Coulon M** (1992) La distension oligocène dans le nord-est du bassin de Paris (perturbation des directions d'extension et distribution des stylolites). *Bulletin de la Société géologique de France* **163**, 531–40.
- Coulon M and Frizon de Lamotte D** (1988) Les craies éclatées du secteur d'Omey (Marne, France); le résultat d'une breccification par fracturation hydraulique en contexte extensif. *Bulletin de la Société géologique de France* **4**, 177–85.
- Cruset D, Vergés J, Albert R, Gerdes A, Benedicto A, Cantarero I and Travé A** (2020) Quantifying deformation processes in the SE Pyrenees using U–Pb dating of fracture-filling calcites. *Journal of the Geological Society, London* **177**, 1186–96.
- Dennis KJ, Affek HP, Passey BH, Schrag DP and Eiler JM** (2011) Defining an absolute reference frame for 'clumped' isotope studies of CO₂. *Geochimica et Cosmochimica Acta* **75**, 7117–31.
- Dèzes P, Schmid SM and Ziegler PA** (2004) Evolution of the European Cenozoic Rift System: interaction of the Alpine and Pyrenean orogens with their foreland lithosphere. *Tectonophysics* **389**, 1–33.
- Durllet C and Thierry J** (2000) Modalités séquentielles de la transgression aaleno-bajocienne sur le sud-est du Bassin parisien. *Bulletin de la Société géologique de France* **171**, 327–39.
- Ge S and Garven G** (1992) Hydromechanical modeling of tectonically driven groundwater flow with application to the Arkoma Foreland Basin. *Journal of Geophysical Research* **97**, 9119–44.
- Goldstein RH and Reynolds TJ** (1994) *Systematics of Fluid Inclusions in Diagenetic Minerals*. SEPM Short Course No. 31. Tulsa: SEPM (Society for Sedimentary Geology).
- Grool AR, Ford M, Vergés J, Huismans RS, Christophoul F and Dielforder A** (2018) Insights into the crustal-scale dynamics of a doubly vergent orogen from a quantitative analysis of its forelands: a case study of the Eastern Pyrenees. *Tectonics* **37**, 450–76.
- Guillocheau F, Robin C, Allemand P, Bourquin S, Brault N, Dromart G, Friedenbergh R, Garcia J-P, Gaulier J-M, Gaumet F, Grosdoy B, Hanot F, Le Strat P, Mettraux M, Nalpas T, Prijac C, Rigoltet C, Serrano O and Grandjean G** (2000) Meso-Cenozoic geodynamic evolution of the Paris Basin: 3D stratigraphic constraints. *Geodinamica Acta* **13**, 189–245.
- Hansman RJ, Albert R, Gerdes A and Ring U** (2018) Absolute ages of multiple generations of brittle structures by U–Pb dating of calcite. *Geology* **46**, 207–10.
- Hill CA, Polyak VJ, Asmerom Y and Provencio P** (2016) Constraints on a Late Cretaceous uplift, denudation, and incision of the Grand Canyon region, southwestern Colorado Plateau, USA, from U–Pb dating of lacustrine limestone. *Tectonics* **35**, 896–906.

- Hoareau G, Crognier N, Lacroix B, Aubourg C, Roberts NMW, Niemi N, Branellec M, Beaudoin N and Suárez Ruiz I (2021) Combination of $\Delta 47$ and U–Pb dating in tectonic calcite veins unravel the last pulses related to the Pyrenean Shortening (Spain). *Earth and Planetary Science Letters* **553**, 116636. doi: [10.1016/j.epsl.2020.116636](https://doi.org/10.1016/j.epsl.2020.116636).
- Homberg C, Bergerat F, Philippe Y, Lacombe O and Angelier J (2002) Structural inheritance and Cenozoic stress fields in the Jura fold-and-thrust belt (France). *Tectonophysics* **357**, 137–58.
- Lacombe O, Angelier J, Bergerat F and Laurent P (1990) Tectoniques superposées et perturbations de contrainte dans la zone transformante Rhin-Saone; apport de l'analyse des failles et des macles de la calcite. *Bulletin de la Société géologique de France* **6**, 853–63.
- Lacombe O, Angelier J, Laurent Ph, Bergerat F and Tournet Ch (1990) Joint analyses of calcite twins and fault slips as a key for deciphering poly-phase tectonics: Burgundy as a case study. *Tectonophysics* **182**, 279–300.
- Lacombe O, Laurent P and Rocher M (1996) Magnitude de la contrainte déviatorique pyrénéenne dans l'avant-pays nord-pyrénéen. *Comptes Rendus de l'Académie des Sciences: Série 2, Earth and Planetary Sciences* **322**, 229–35.
- Lacombe O and Mouthereau F (1999) Qu'est-ce que le front des orogènes ? L'exemple de l'orogène pyrénéen. *Comptes Rendus de l'Académie des Sciences: Série 2, Earth and Planetary Sciences* **329**, 889–96.
- Lacombe O and Obert D (2000) Héritage structural et déformation de couverture: plissement et fracturation tertiaires dans l'Ouest du bassin de Paris. *Comptes Rendus de l'Académie des Sciences – Series IIA – Earth and Planetary Science* **330**, 793–8.
- Lawson M, Shenton BJ, Stolper DA, Eiler JM, Rasbury ET, Becker TP, Phillips-Lander CM, Buono AS, Becker SP, Pottorf R, Gray GG, Yurewicz D and Gournay J (2018) Deciphering the diagenetic history of the El Abra Formation of eastern Mexico using reordered clumped isotope temperatures and U–Pb dating. *Geological Society of America Bulletin* **130**, 617–29.
- Lefort A, Lathuilière B, Carpentier C and Huault V (2011) Microfossil assemblages and relative sea-level fluctuations in a lagoon at the Oxfordian/Kimmeridgian boundary (Upper Jurassic) in the eastern part of the Paris Basin. *Facies* **57**, 649–62.
- Lenoir L, Blaise T, Somogyi A, Brigaud B, Barbarand J, Boukari C, Nouet J, Brézard-Oudot A and Pagel M (2021) Uranium incorporation in fluorite and exploration of U–Pb dating. *Geochronology* **3**, 199–227. doi: [10.5194/gchron-3-199-2021](https://doi.org/10.5194/gchron-3-199-2021).
- Le Roux J (1980) La tectonique de l'aureole orientale du bassin de Paris; ses relations avec la sédimentation. *Bulletin de la Société géologique de France* **22**, 655–62.
- Letouzey J (1986) Cenozoic paleo-stress pattern in the Alpine Foreland and structural interpretation in a platform basin. *Tectonophysics* **132**, 215–31.
- Macchiavelli C, Vergés J, Schettino A, Fernández M, Turco E, Casciello E, Torne M, Pierantoni PP and Tunini L (2017) A new southern North Atlantic isochron map: insights into the drift of the Iberian plate since the Late Cretaceous: Iberian plate kinematics since 83.5 Ma. *Journal of Geophysical Research: Solid Earth* **122**, 9603–26.
- Malfilatre C, Boulvais P, Dabard M-P, Bourquin S, Hallot E, Pallix D and Gapais D (2012) Petrographical and geochemical characterization of Comblanchien limestone (Bourgogne, France): a fingerprint of the building stone provenance. *Comptes Rendus Geoscience* **344**, 14–24.
- Mangenot X, Gasparini M, Gerdes A, Bonifacie M and Rouchon V (2018) An emerging thermochronometer for carbonate-bearing rocks: $\Delta 47$ /(U–Pb). *Geology* **46**, 1067–70.
- Mazurek M, Davis DW, Madritsch H, Rufer D, Villa IM, Sutcliffe CN, de Haller A and Traber D (2018) Veins in clay-rich aquitards as records of deformation and fluid-flow events in northern Switzerland. *Applied Geochemistry* **95**, 57–70.
- Mouthereau F, Angrand P, Jourdon A, Ternois S, Fillon C, Calassou S, Chevrot S, Ford M, Jolivet L, Manatschal G, Masini E, Thion I, Vidal O and Baudin T (2021) Cenozoic mountain building and topographic evolution in Western Europe: impact of billions of years of lithosphere evolution and plate kinematics. *BSGF – Earth Sciences Bulletin* **192**, 56. doi: [10.1051/bsgf/2021040](https://doi.org/10.1051/bsgf/2021040).
- Nuriel P, Weinberger R, Kylander-Clark ARC, Hacker BR and Craddock JP (2017) The onset of the Dead Sea transform based on calcite age-strain analyses. *Geology* **45**, 587–90.
- Olivier N, Carpentier C, Martin-Garin B, Lathuilière B, Gaillard C, Ferry S, Hantzpergue P and Geister J (2004) Coral-microbialite reefs in pure carbonate versus mixed carbonate-siliciclastic depositional environments: the example of the Pagny-sur-Meuse section (Upper Jurassic, northeastern France). *Facies* **50**, 229–55.
- O'Neil JR, Clayton RN and Mayeda TK (1969) Oxygen isotope fractionation in divalent metal carbonates. *Journal of Chemical Physics* **51**, 5547–57.
- Pagel M, Bonifacie M, Schneider DA, Gautheron C, Brigaud B, Calmels D, Cros A, Saint-Bezar B, Landrein P, Sutcliffe C, Davis D and Chaduteau C (2018) Improving paleohydrological and diagenetic reconstructions in calcite veins and breccia of a sedimentary basin by combining $\Delta 47$ temperature, $\delta^{18}\text{O}_{\text{water}}$ and U–Pb age. *Chemical Geology* **481**, 1–17.
- Parizot O, Missenard Y, Barbarand J, Blaise T, Benedicto A, Haurine F and Sarda P (2022) How sensitive are intraplate inherited structures? Insight from the Cévennes Fault System (Languedoc, SE France). *Geological Magazine*, published online 11 April 2022. doi: [10.1017/S0016756822000152](https://doi.org/10.1017/S0016756822000152).
- Parizot O, Missenard Y, Haurine F, Blaise T, Barbarand J, Benedicto A and Sarda P (2021) When did the Pyrenean shortening end? Insight from U–Pb geochronology of syn-faulting calcite (Corbières area, France). *Terra Nova* **33**, 551–9.
- Parrish RR, Parrish CM and Lasalle S (2018) Vein calcite dating reveals Pyrenean orogen as cause of Paleogene deformation in southern England. *Journal of the Geological Society, London* **175**, 425–42.
- Passey BH, Levin NE, Cerling TE, Brown FH and Eiler JM (2010) High-temperature environments of human evolution in East Africa based on bond ordering in paleosol carbonates. *Proceedings of the National Academy of Sciences of the United States of America* **107**, 11245–9. doi: [10.1073/pnas.1001824107](https://doi.org/10.1073/pnas.1001824107).
- Paton C, Hellstrom J, Paul B, Woodhead J and Hergt J (2011) Iolite: freeware for the visualisation and processing of mass spectrometric data. *Journal of Analytical Atomic Spectrometry* **26**, 2508. doi: [10.1039/C1JA10172B](https://doi.org/10.1039/C1JA10172B).
- Pisapia C, Deschamps P, Battani A, Buschaert S, Guihou A, Hamelin B and Brulhet J (2018) U/Pb dating of geodic calcite: new insights on Western Europe major tectonic events and associated diagenetic fluids. *Journal of the Geological Society, London* **175**, 60–70.
- Ring U and Gerdes A (2016) Kinematics of the Alpenrhein-Bodensee graben system in the Central Alps: Oligocene/Miocene transtension due to formation of the Western Alps arc: Alpenrhein-Bodensee graben system. *Tectonics* **35**, 1367–91.
- Roberts NMW and Holdsworth RE (2022) Timescales of faulting through calcite geochronology: a review. *Journal of Structural Geology* **158**, 104578. doi: [10.1016/j.jsg.2022.104578](https://doi.org/10.1016/j.jsg.2022.104578).
- Roberts NMW, Lee JK, Holdsworth RE, Jeans C, Farrant AR and Haslam R (2020) Near-surface Palaeocene fluid flow, mineralisation and faulting at Flamborough Head, UK: new field observations and U–Pb calcite dating constraints. *Solid Earth* **11**, 1931–45.
- Roberts NMW, Rasbury ET, Parrish RR, Smith CJ, Horstwood MSA and Condon DJ (2017) A calcite reference material for LA-ICP-MS U–Pb geochronology. *Geochemistry, Geophysics, Geosystems* **18**, 2807–14.
- Rocher M, Cushing M, Lemeille F, Lozac'h Y and Angelier J (2004) Intraplate paleostresses reconstructed with calcite twinning and faulting: improved method and application to the eastern Paris Basin (Lorraine, France). *Tectonophysics* **387**, 1–21.
- Sibson H (1994) Crustal stress, faulting and fluid flow. In *Geofluids: Origin, Migration and Evolution of Fluids in Sedimentary Basins* (ed. J Parnell), pp. 69–84. Geological Society of London, Special Publication no. 78.
- Smeraglia L, Looser N, Fabbri O, Choulet F, Guillong M and Bernasconi SM (2021) U–Pb dating of middle Eocene–Pliocene multiple tectonic pulses in the Alpine foreland. *Solid Earth* **12**, 2539–51.

- Sun X, Gomez-Rivas E, Cruset D, Alcalde J, Muñoz-Lopez D, Cantarero I, Martin-Martin JD, John CM and Travé A** (2022) Origin and distribution of calcite cements in a folded fluvial succession: the Puig-reig anticline (south-eastern Pyrenees). *Sedimentology* **69**, 2319–47.
- Sutcliffe CN, Thibodeau AM, Davis DW, Al-Aasm I, Parmenter A, Zajacz Z and Jensen M** (2020) Hydrochronology of a proposed deep geological repository for low- and intermediate-level nuclear waste in southern Ontario from U–Pb dating of secondary minerals: response to Alleghanian events. *Canadian Journal of Earth Sciences* **57**, 494–505.
- Swart PK, Burns SJ and Leder JJ** (1991) Fractionation of the stable isotopes of oxygen and carbon in carbon dioxide during the reaction of calcite with phosphoric acid as a function of temperature and technique. *Chemical Geology: Isotope Geoscience Section* **86**, 89–96.
- Vandeginste V, Swennen R, Allaeyns M, Ellam RM, Osadetz K and Roure F** (2012) Challenges of structural diagenesis in foreland fold-and-thrust belts: a case study on paleofluid flow in the Canadian Rocky Mountains West of Calgary. *Marine and Petroleum Geology* **35**, 235–51.
- Vermeesch P** (2018) IsoplotR: a free and open toolbox for geochronology. *Geoscience Frontiers* **9**, 1479–93.
- Villemin T** (1986) La chronologie des événements tectoniques dans le Nord-Est de la France et le Sud-Ouest de l'Allemagne du Permien à l'Actuel. *Comptes Rendus de l'Académie des Sciences de Paris* **303**, 1685–90.
- Vincent B, Emmanuel L, Houel P and Loreau J-P** (2007) Geodynamic control on carbonate diagenesis: petrographic and isotopic investigation of the Upper Jurassic formations of the Paris Basin (France). *Sedimentary Geology* **197**, 267–89.
- Woodhead JD, Horstwood MSA and Cottle P** (2016) Advances in isotope ratio determination by LA–ICP–MS. *Elements* **12**, 317–22.
- Ziegler PA** (1987) Late Cretaceous and Cenozoic intra-plate compressional deformations in the Alpine foreland—a geodynamic model. *Tectonophysics* **137**, 389–420.
- Ziegler PA** (1990) *Geological Atlas of Western and Central Europe*. The Hague: Shell Internationale Petroleum Maatschappij B.V.
- Ziegler PA and Dèzes P** (2007) Cenozoic uplift of Variscan Massifs in the Alpine foreland: timing and controlling mechanisms. *Global and Planetary Change* **58**, 237–69.